Pattern selection in oscillatory longwave Marangoni convection with nonlinear temperature dependence of surface tension

Alexander B. Mikishev [*]
Department of Engineering Technology, Sam Houston State University, Huntsville, Texas 77341, USA

Alexander A. Nepomnyashchy [†]
Department of Mathematics, Technion-Israel Institute of Technology, Haifa 32000, Israel

(Received 10 September 2020; accepted 5 January 2021; published 19 January 2021)

Three-dimensional (3D) longwave oscillatory Marangoni convection in a heated thin layer with weak heat flux from the free surface is considered. Numerous experiments show that the surface tension is a nonlinear function of temperature. Here we modify the system of nonlinear longwave evolution equations expanding the temperature coefficient of the surface tension into the Taylor series about the surface temperature. Using the weakly nonlinear analysis we explore the patterns formed near the critical value of Marangoni number. Stability of the 3D patterns on square, rhombic, and hexagonal lattices are considered. The nonlinearity of the surface tension's temperature dependence can be a stabilizing factor as well as destabilizing one.

DOI: 10.1103/PhysRevFluids.6.014002

I. INTRODUCTION

Pattern formation is a topical subject of investigation in various dissipative systems outside the thermodynamic equilibrium [1]. In fluid dynamics the competition between disturbances may generate different spatial structures and lead to their interesting evolution dynamics, especially in the rich problem for the oscillatory instability mode. Pattern formation and selection are in a focus in exploration of Rayleigh-Bénard convection [2], magnetohydrodynamics [3], ferrofluids [4], binary fluids [5], granular flows [6], and biological systems [7].

One of the most important hydrodynamic phenomena generating patterns is Marangoni convection. This surface-tension-driven convection is a subject of intensive research over the past decades, because of technological progress. Investigation of Marangoni patterns was started by Scanlon and Segel [8]. They considered the patterns generated by a short-wave monotonic instability in a horizontal layer heated from below. There exist also two kinds of *longwave monotonic* instabilities, (i) in the case of poorly conducting boundaries (the mode of Pearson) [9] and (ii) in the case of a thin film (the mode of Scriven and Sternling [10]). The development of a longwave instability is characterized by the existence of slowly evolving "active" variables that determine the nonlinear dynamics; other variables are "enslaved" to them. The investigation of pattern formation in the case of the Pearson's mode, where the active variable is the temperature, was started by Sivashinsky [11] and Knobloch [12]. The nonlinear development of the mode of Scriven and Sternling, where the active variable is the free-surface deformation, was studied by Davis [13]. Golovin *et al.* [14] considered the joint action of both instability modes. Recently, Shklyaev *et al.* [15] found that the

[*]Corresponding author: amik@shsu.edu
[†]nepom@technion.ac.il

 ©2021 American Physical Society

interaction of the temperature disturbance and the surface deformation can create an *oscillatory* instability.

A majority of the theoretical works devoted to the Marangoni pattern formation are based on the assumption of linear dependence of the surface tension function on temperature. However, a lot of experimental data indicate more complicated dependence [16–21]. Our previous paper [22] shows that nonlinearity of the surface tension's temperature dependence can be a stabilizing factor as well as destabilizing one, depending on the kind of patterns.

In the present work, we study how the nonlinear dependence of the surface tension on temperature influences the bifurcation and stability of spatially periodic wave patterns generated by the longwave oscillatory Marangoni instability with a wave number $k \sim \mathrm{Bi}^{1/2}$ (Bi is the Biot number) in a thin layer of liquid with deformable poorly conducting interface. The analysis of bifurcations is performed on square, rhombic, and hexagonal lattices in Fourier space.

II. FORMULATION OF THE PROBLEM (LONG-WAVE APPROACH)

Let us consider a three-dimensional (3D) liquid layer of the mean thickness d_0 heated from below with deformable free surface $z = H(x, y, t)$. We assume that the heat flux at the bottom $Q > 0$ is fixed, and in the absence of convection a vertical temperature gradient $-a = -Q/\lambda < 0$ is created, where λ is the heat conductivity of the liquid. Here we use the fact that, if the heat conductivity of the substrate is low compared to the heat conductivity of the liquid, the heat flux on the bottom is nearly constant, and its distribances due to the convection in the liquid are negligible [23]. The z axis is directed vertically upward, and the (x, y) plane is perpendicular to z axis. The liquid is characterized by the kinematic viscosity ν, the thermal diffusivity χ, the density ρ, the dynamic viscosity $\eta = \nu\rho$, and the heat transfer coefficient at the free surface q. The surface tension $\sigma = \sigma(T)$ is a function of temperature specified later.

To formulate the problem in nondimensional variables, we use the following scales: length d_0, time d_0^2/χ, velocity χ/d_0, temperature ad_0, and pressure $\rho\nu\chi/d_0^2$ and the following parameters: $G = gd_0^3/\nu\chi$ is the modified Galileo number, $S = \sigma d_0/\chi\eta$ is the inverse capillary number, $\mathrm{Bi} = qd_0/\lambda$ is the Biot number, and $M = -\sigma_T Q d_0^2/(\lambda\eta\chi)$ is the Marangoni number, where $\sigma_T = d\sigma(T)/dT$ is a function of the surface temperature $T|_{z=H}$.

The equations governing the large-scale Marangoni convection are derived from the basic equations of viscous fluid dynamics and heat transfer by rescaling of coordinates

$$X = \epsilon x, \quad Y = \epsilon y, \quad Z = z$$

and the time

$$\tau = \epsilon^2 t.$$

Here parameter $\epsilon \ll 1$ can be defined as a ratio between the layer mean thickness d_0 and typical horizontal scale of the problem. The appropriate scaling of the inverse capillary parameter for our problem is $S = \epsilon^{-2}\Sigma$ and the Biot number is $\mathrm{Bi} = \epsilon^2\beta$. The applied scaling corresponds to the consideration of disturbances with the wave number $k \sim \epsilon$, i.e., $k \sim \mathrm{Bi}^{1/2}$. By means of the asymptotic expansions [15], the problem is reduced to a system of coupled equations governing the evolution of *active variables*, the local film thickness $H(X, Y, \tau)$, and the bottom temperature deviation $F(X, Y, \tau)$:

$$\partial_\tau H = \nabla \cdot \left(\frac{H^3}{3} \nabla R + \frac{M(\Theta) H^2}{2} \nabla\Theta \right) \equiv \nabla \cdot \mathbf{Q_1}, \tag{1}$$

$$H\partial_\tau F = \nabla \cdot \left(\frac{H^4}{8} \nabla R + \frac{M(\Theta) H^3}{6} \nabla\Theta + H\nabla F \right) + \mathbf{Q_1} \cdot \nabla\Theta - \frac{1}{2}(\nabla H)^2 - \beta\Theta, \tag{2}$$

where $R = GH - \Sigma\nabla^2 H$ is a pressure disturbance, $\Theta = F - H$ is the surface temperature deviation, $\nabla = (\partial/\partial X, \partial/\partial Y)$. The vector $-\mathbf{Q_1}$ has a meaning of the longitudinal flux of a liquid integrated across the layer.

The Marangoni number depends on the temperature coefficient of the surface tension σ_T that is a function of the temperature at the interface.

Equations (1) and (2) have a base solution, $H^{(b)} = 1$, $F^{(b)} = 1$, hence $\Theta^{(b)} = 0$.

In this work we consider the nonlinear evolution of large-scale perturbations near the critical Marangoni number of the oscillatory instability mode, which corresponds to the minimum m_0 of the oscillatory neutral curve

$$M_o^{(b)}(K) = 3 + 3\beta/K^2 + G + \Sigma K^2, \tag{3}$$

obtained by solving the linear instability problem in Ref. [15]. Here $K = k/\epsilon \sim O(1)$ is the rescaled wave number. The minimum value of Marangoni number is reached at $K_c^o = (3\beta/\Sigma)^{1/4}$.

We expand the Marangoni number into Taylor series around the undisturbed temperature value of the free surface, i.e.,

$$M(\Theta) = m_0^* + m_1\Theta + m_2\Theta^2 + \ldots, \tag{4}$$

where m_0^* is the Marangoni number in the motionless state, $m_1 = dM/d\Theta$, $m_2 = (1/2)d^2M/d\Theta^2$, etc.

The nonlinear evolution is considered near the instability threshold, therefore, we suppose $|m_0^* - m_0| \ll 1$, where m_0^* is the actual Marangoni number and m_0 is the critical Marangoni number for oscillatory instability. For the variables H and F we introduce the expansion in powers of small parameter δ:

$$H = 1 + \delta h_1 + \delta^2 h_2 + \ldots, \tag{5}$$

$$F = 1 + \delta f_1 + \delta^2 f_2 + \ldots. \tag{6}$$

Taking these expansions into account, for the Marangoni number we obtain the following expansion:

$$M = m_0^* + \delta m_1(f_1 - h_1) + \delta^2[m_1(f_2 - h_2) + m_2(f_1 - h_1)^2] + \ldots. \tag{7}$$

Also, we separate the fast oscillations depending on time $\tau_0 = \tau$ and the slow nonlinear evolution of the amplitudes of perturbations characterized by the time scale $\tau_2 = \delta^2\tau$. The time derivative is presented as

$$\partial_\tau = \partial_{\tau_0} + \delta^2\partial_{\tau_2} + \ldots.$$

As shown in Ref. [15], the formation of the wave patterns is a result of a Hopf bifurcation, so we introduce $m_0^* = m_0 + \delta^2 m_{02}$ in Eq. (7).

A. Square and Roll Patterns

Substituting Eqs. (5)–(7) into Eqs. (1) and (2) and collecting terms of the same order we obtain the following at the leading order:

$$h_{1,\tau_0} = \frac{1}{3}\nabla^2 R_1 + \frac{m_0}{2}\nabla^2(f_1 - h_1), \tag{8}$$

$$f_{1,\tau_0} = \nabla^2\left[\frac{1}{8}R_1 + \frac{m_0}{6}(f_1 - h_1) + f_1\right] - \beta(f_1 - h_1), \tag{9}$$

where $R_1 = Gh_1 - \Sigma\nabla^2 h_1$.

We present the solution of Eqs. (8) and (9) for the *square lattice* in the form

$$h_1 = A_1 e^{iKX + i\omega_0\tau_0} + A_2 e^{-iKX + i\omega_0\tau_0} + B_1 e^{iKY + i\omega_0\tau_0} + B_2 e^{-iKY + i\omega_0\tau_0} + \text{c.c.} \tag{10}$$

$$f_1 = \alpha(A_1 e^{iKX + i\omega_0\tau_0} + A_2 e^{-iKX + i\omega_0\tau_0} + B_1 e^{iKY + i\omega_0\tau_0} + B_2 e^{-iKY + i\omega_0\tau_0}) + \text{c.c.} \tag{11}$$

Here $\alpha = 1 - 2(G + k^2\Sigma)/3m_0 - 2i\omega_0/m_0K^2$.

At the second order we obtain

$$h_{2,\tau_0} - \nabla^2\left[\frac{1}{3}R_2 + \frac{m_0}{2}(f_2 - h_2)\right] = \nabla\cdot\left[h_1\nabla R_1 + m_0 h_1\nabla(f_1 - h_1) + \frac{m_1}{2}(f_1 - h_1)\nabla(f_1 - h_1)\right], \tag{12}$$

$$\begin{aligned} &f_{2,\tau_0} - \nabla^2\left[f_2 + \frac{1}{8}R_2 + \frac{m_0}{6}(f_2 - h_2)\right] + \beta(f_2 - h_2) \\ &\quad = -h_1 f_{1,\tau_0} + \nabla(h_1\nabla f_1) - \frac{1}{2}(\nabla h_1)^2 + \frac{1}{2}\nabla(h_1\nabla R_1) + \frac{1}{3}\nabla(f_1 - h_1)\nabla R_1 \\ &\qquad + \frac{m_0}{2}[\nabla f_1\nabla(f_1 - h_1) + h_1\nabla^2(f_1 - h_1)] + \frac{m_1}{6}\nabla[(f_1 - h_1)\nabla(f_1 - h_1)]. \end{aligned} \tag{13}$$

Here $R_2 = Gh_2 - \Sigma\nabla^2 h_2$. We search the solution at the second order in the form

$$\begin{aligned} h_2 = {} & C_1 e^{2iKX} + C_2 e^{2iKY} + C_3 e^{2iKX+2i\omega_0\tau_0} + C_4 e^{-2iKX+2i\omega_0\tau_0} + C_5 e^{iKX+iKY+2i\omega_0\tau_0} \\ & + C_6 e^{2iKY+2i\omega_0\tau_0} + C_7 e^{-iKX+iKY+2i\omega_0\tau_0} + C_8 e^{iKX-iKY+2i\omega_0\tau_0} + C_9 e^{-iKX-iKY+2i\omega_0\tau_0} \\ & + C_{10} e^{-2iKY+2i\omega_0\tau_0} + C_{11} e^{iKX+iKY} + C_{12} e^{-iKX+iKY} + \text{c.c.}, \end{aligned} \tag{14}$$

$$\begin{aligned} f_2 = {} & F_0 + F_1 e^{2i\omega_0\tau_0} + D_1 e^{2iKX} + D_2 e^{2iKY} + D_3 e^{2iKX+2i\omega_0\tau_0} + D_4 e^{-2iKX+2i\omega_0\tau_0} \\ & + D_5 e^{iKX+iKY+2i\omega_0\tau_0} + D_6 e^{2iKY+2i\omega_0\tau_0} + D_7 e^{-iKX+iKY+2i\omega_0\tau_0} + D_8 e^{iKX-iKY+2i\omega_0\tau_0} \\ & + D_9 e^{-iKX-iKY+2i\omega_0\tau_0} + D_{10} e^{-2iKY+2i\omega_0\tau_0} + D_{11} e^{iKX+iKY} + D_{12} e^{-iKX+iKY} + \text{c.c.} \end{aligned} \tag{15}$$

Using the solvability conditions for the system at the third order we obtain the following system of the Landau equations for amplitudes A_j and B_j ($j = 1, 2$):

$$\frac{dA_1}{d\tau_2} = (\kappa_0 + \kappa_1|A_1|^2 + \kappa_2|A_2|^2)A_1 + \kappa_3(|B_1|^2 + |B_2|^2)A_1 + \kappa_4 A_2^* B_1 B_2, \tag{16}$$

$$\frac{dA_2}{d\tau_2} = (\kappa_0 + \kappa_1|A_2|^2 + \kappa_2|A_1|^2)A_2 + \kappa_3(|B_1|^2 + |B_2|^2)A_2 + \kappa_4 A_1^* B_1 B_2, \tag{17}$$

$$\frac{dB_1}{d\tau_2} = (\kappa_0 + \kappa_1|B_1|^2 + \kappa_2|B_2|^2)B_1 + \kappa_3(|A_1|^2 + |A_2|^2)B_1 + \kappa_4 B_2^* A_1 A_2, \tag{18}$$

$$\frac{dB_2}{d\tau_2} = (\kappa_0 + \kappa_1|B_2|^2 + \kappa_2|B_1|^2)B_2 + \kappa_3(|A_1|^2 + |A_2|^2)B_2 + \kappa_4 B_1^* A_1 A_2. \tag{19}$$

The coefficients κ_j ($j = 0, \ldots, 4$) are complex, and they can be presented as $\kappa_j = \kappa_{j,r} + i\kappa_{j,i}$. For example,

$$\kappa_0 = \left(\frac{K^2}{6} - i\frac{K^4(G + \Sigma K^2 + 72)}{288\omega_0}\right)m_{0,2}. \tag{20}$$

Other coefficients are cumbersome to be given here. They are given in the Supplemental Material [24].

The nonlinear forms of amplitude Eqs. (16)–(19) are determined by the invariance of the equations under X translation, Y translation, τ translation, X reflection, Y reflection, and rotation through $\pi/2$. The system of Eqs. (16)–(19) was considered in detail by Silber and Knobloch in Ref. [25], where the authors found, beside the trivial solution with all amplitudes equal to zero, the symmetric solutions; see Table I.

The patterns on the square lattice can be stable if they emerge through the direct Hopf bifurcation ($\kappa_{0,r} > 0$). Other stability conditions are obtained in Ref. [25]. The stability conditions for these solutions are the following:

(i) TR: $\kappa_{1,r} < 0, \kappa_{2,r} - \kappa_{1,r} < 0, \kappa_{3,r} - \kappa_{1,r} < 0$;

(ii) SR: $\kappa_{1,r} + \kappa_{2,r} < 0, \kappa_{1,r} - \kappa_{2,r} < 0, 2\kappa_{3,r} - \kappa_{1,r} - \kappa_{2,r} < 0, |\kappa_4|^2 - |2\kappa_3 - (\kappa_1 + \kappa_2)|^2 < 0$;

TABLE I. The symmetric solutions of Eqs. (16)–(19) found in Ref. [25].

(i) Traveling rolls (TR)	$\lvert A_1\rvert^2 = -\kappa_{0,r}/\kappa_{1,r}, A_2 = B_1 = B_2 = 0$
(ii) Standing rolls (SR)	$A_1 = A_2 \neq 0, \lvert A_1\rvert^2 = -\kappa_{0,r}/(\kappa_{1,r} + \kappa_{2,r}), B_1 = B_2 = 0$
(iii) Traveling squares (TS)	$A_1 = B_1 \neq 0, \lvert A_1\rvert^2 = -\kappa_{0,r}/(\kappa_{1,r} + \kappa_{3,r}), A_2 = B_2 = 0$
(iv) Standing squares (SS)	$A_1 = A_2 = B_1 = B_2 \neq 0,$ $\lvert A_1\rvert^2 = -\kappa_{0,r}/(\kappa_{1,r} + \kappa_{2,r} + 2\kappa_{3,r} + \kappa_{4,r})$
(v) Alternating rolls (AR)	$A_1 = A_2 = iB_1 = iB_2 \neq 0,$ $\lvert A_1\rvert^2 = -\kappa_{0,r}/(\kappa_{1,r} + \kappa_{2,r} + 2\kappa_{3,r} - \kappa_{4,r})$
(vi) Standing cross rolls (SCR)	$A_1 = A_2 \neq 0, B_1 = B_2 \neq 0, \lvert A_1\rvert \neq \lvert B_1\rvert$

(iii) TS: $\kappa_{1,r} + \kappa_{3,r} < 0, \kappa_{1,r} - \kappa_{3,r} < 0, \kappa_{2,r} - \kappa_{1,r} + \kappa_{4,r} < 0, \kappa_{2,r} - \kappa_{1.r} - \kappa_{4,r} < 0;$
(iv) SS: $\kappa_{1,r} + \kappa_{2,r} + 2\kappa_{3,r} + \kappa_{4,r} < 0, \kappa_{1,r} - \kappa_{2,r} - \kappa_{4,r} < 0,$
$\kappa_{1,r} + \kappa_{2,r} - 2\kappa_{3,r} - 3\kappa_{4,r} < 0, \mathrm{Re}[\kappa_{4,i}(\kappa_1 + \kappa_2 - 2\kappa_3)] - \lvert\kappa_4\rvert^2 < 0;$
(v) AR: $\kappa_{1,r} + \kappa_{2,r} + 2\kappa_{3,r} - \kappa_{4,r} < 0, \kappa_{1,r} + \kappa_{2,r} - 2\kappa_{3,r} + 3\kappa_{4,r} < 0,$
$\kappa_{1,r} - \kappa_{2,r} + \kappa_{4,r} < 0, -\lvert\kappa_{4,r}\rvert^2 - \mathrm{Re}[\kappa^*_{4,r}(\kappa_{1,r} + \kappa_{2,r} - 2\kappa_{3,r})] < 0.$

The SCR-solution is out of our scope, because as shown in Ref. [25] this pattern is always unstable.

We did not find numerically stability domains for SR-, TS-, and SS-solution for the oscillatory Marangoni convection. The regions of stable TR solution were found and described in our previous work [22]. Here we in details consider the AR-solution for different surface tension functions. The calculations are performed with $\Sigma = 1$. Note that obtained results can be used for arbitrary values of Σ with an appropriate rescaling of β.

The results of calculation are shown in Fig. 1. Here together with domains of stable AR solution the regions of stable TR solution are drawn. When the surface tension function is a linear function of temperature ($m_1 = 0, m_2 = 0$), Fig. 1(a), the AR solution is stable in a small region to the left of the red dashed line (these are results of Shklyaev *et al.*, see Ref. [15]). In the case of the nonlinear surface tension the region of the stable AR expands or shrinks depending on the values of the coefficients m_1 and m_2. The "blue sector" in Fig. 1(b) is for $m_1 = 0.6m_0$ and $m_2 = 0$, the "brown sector" [Fig. 1(c)] is for $m_1 = -0.5m_0$ and $m_2 = 0$, and the "purple sector" [Fig. 1(d)] is for $m_1 = 0.8m_0$ and $m_2 = -0.3m_0$. Here $m_0 = m_{\mathrm{osc}}(K_c^0)$ and its values are positive, however, values of m_1 and m_2 can be both positive and negative. Parameters m_1 and m_2 are taken mainly from experimental data [17,18,21]. The data were obtained investigating the properties of diluted aqueous solutions of h-heptanol (6×10^{-2} molal) and of n-hexanol (4×10^{-2} molal), or long chain alcohol solutions with six and nine carbon atoms. The graphs in the papers were digitilized and fitted by empirical law as a surface tension function of temperature.

The calculation shows that in the cases (a) and (b) the AR and TR domains overlap forming a small region of *bistability* denoted in the figure as "AR & TR," Fig. 1(e). In this region both solutions are stable. The existence of the "AR & TR" region depends on the nonlinearity of the surface tension function.

B. Rhombic patterns

Now we consider the pattern selection on rhombic lattice. Here we construct solutions at the leading order system Eqs. (8) and (9) in the following form:

$$h_1 = [A_1 e^{iKX} + A_2 e^{-iKX} + B_1 e^{iKX\cos(\theta) + iKY\sin(\theta)} + B_2 e^{-iKX\cos(\theta) - iKY\sin(\theta)}]e^{i\omega_0\tau_0} + \text{c.c.}, \tag{21}$$

$$f_1 = \alpha[A_1 e^{iKX} + A_2 e^{-iKX} + B_1 e^{iKX\cos(\theta) + iKY\sin(\theta)} + B_2 e^{-iKX\cos(\theta) - iKY\sin(\theta)}]e^{i\omega_0\tau_0} + \text{c.c.} \tag{22}$$

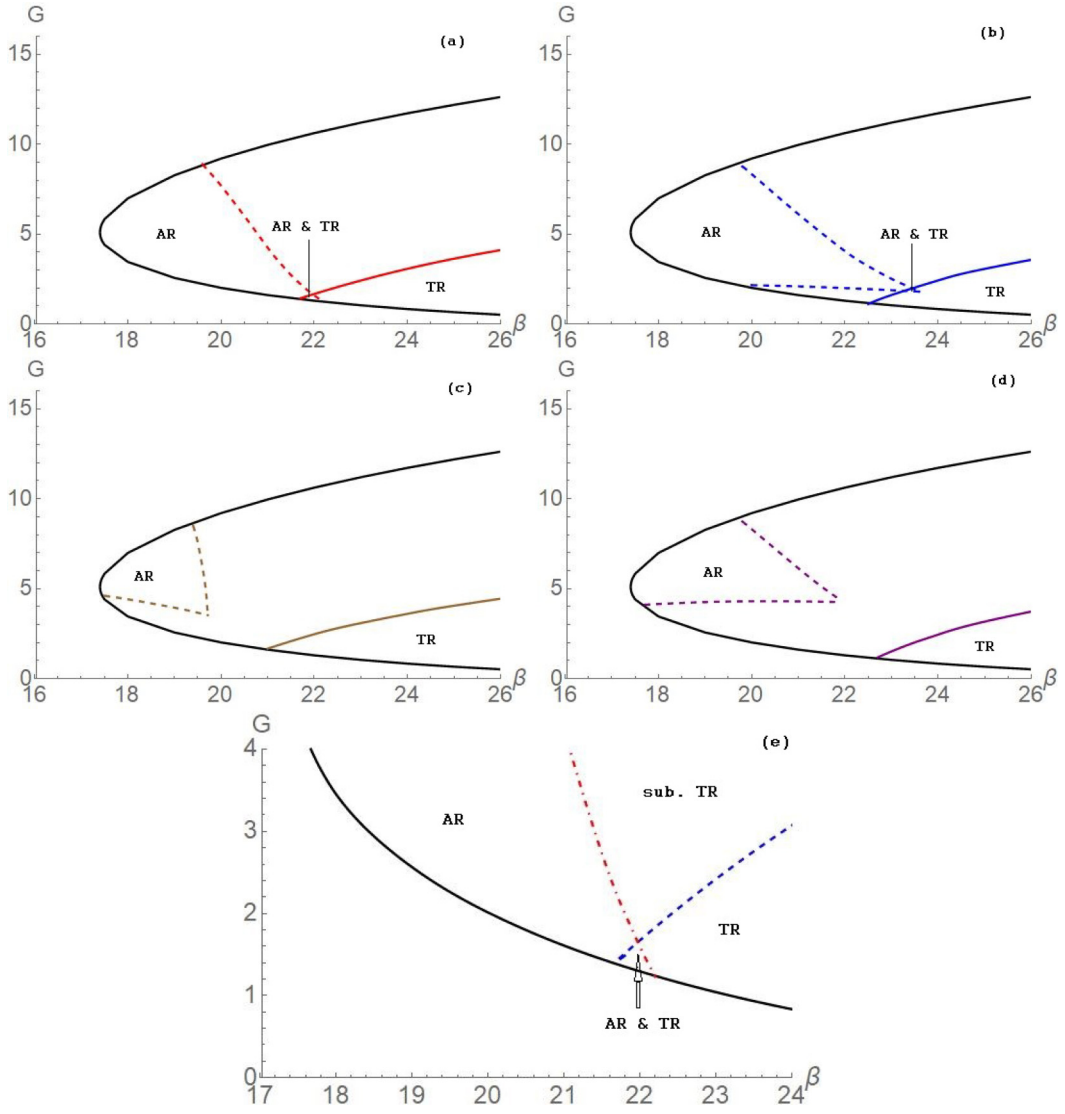

FIG. 1. Pattern selection of oscillatory mode on square lattice. Domains of stability for TR (solid lines) and AR (dashed lines), regions noted as "AR & TR" are regions of bistability. Panels: (a) linear surface tension, results of Shklyaev *et al.* [15]; (b) $m_1 = 0.6m_0$, $m_2 = 0$ (blue color); (c) $m_1 = -0.5m_0$, $m_2 = 0$ (brown color); (d) $m_1 = 0.8m_0$, $m_2 = -0.3m_0$ (purple color). Panel (e) shows zoomed-in bistability domain for linear surface tension function.

The solution is a result of interaction of the waves propagating along the x axis and the waves with wave vectors $\pm K(\cos\theta, \sin\theta)$. The angle θ here plays the role of additional parameter.

Removing singularity on the third order of the solution expansions we obtain the amplitude equations in the form of Landau-Ginzburg equations:

$$\frac{dA_1}{d\tau_2} = (\kappa_0 + \kappa_1|A_1|^2 + \kappa_2|A_2|^2)A_1 + \kappa_5(\theta)|B_1|^2A_1 + \kappa_5'(\theta)|B_2|^2A_1 + \kappa_6(\theta)A_2^*B_1B_2, \quad (23)$$

$$\frac{dA_2}{d\tau_2} = (\kappa_0 + \kappa_1|A_2|^2 + \kappa_2|A_1|^2)A_2 + \kappa_5(\theta)|B_2|^2A_2 + \kappa_5'(\theta)|B_1|^2A_2 + \kappa_6(\theta)A_1^*B_1B_2. \quad (24)$$

By a permutation of A_j and B_j $(j = 1, 2)$ we obtain an additional pair of the equations for amplitudes B_j. Here $\kappa_5'(\theta) = \kappa_5(\pi - \theta)$. Note that the coefficients $\kappa_5(\theta)$ and $\kappa_5'(\theta)$ are equal for many convection problems with nondeformable interface, but it is not our case. Note also that the case of $\theta = \pi/2$ is a case of square lattice.

Using the polar notation for the amplitudes in the system for the amplitude equation, $A_1 = R_1(\tau_2)e^{i\phi_1(\tau_2)}$, $A_2 = R_2(\tau_2)e^{i\phi_2(\tau_2)}$, $B_1 = R_3(\tau_2)e^{i\phi_3(\tau_2)}$, and $B_2 = R_4(\tau_2)e^{i\phi_4(\tau_2)}$, we obtain the following set of equations:

$$\frac{dR_1}{d\tau_2} + iR_1\frac{d\phi_1}{d\tau_2} = \left(\kappa_0 + \kappa_1 R_1^2 + \kappa_2 R_2^2 + \kappa_5 R_3^2 + \kappa_5' R_4^2\right)R_1 + \kappa_6 R_2 R_3 R_4 e^{i\Delta}, \tag{25}$$

$$\frac{dR_2}{d\tau_2} + iR_2\frac{d\phi_2}{d\tau_2} = \left(\kappa_0 + \kappa_1 R_2^2 + \kappa_2 R_1^2 + \kappa_5 R_3^2 + \kappa_5' R_4^2\right)R_2 + \kappa_6 R_1 R_3 R_4 e^{i\Delta}, \tag{26}$$

$$\frac{dR_3}{d\tau_2} + iR_3\frac{d\phi_3}{d\tau_2} = \left(\kappa_0 + \kappa_1 R_3^2 + \kappa_4 R_4^2 + \kappa_5 R_1^2 + \kappa_5' R_2^2\right)R_3 + \kappa_6 R_4 R_1 R_2 e^{-i\Delta}, \tag{27}$$

$$\frac{dR_4}{d\tau_2} + iR_4\frac{d\phi_4}{d\tau_2} = \left(\kappa_0 + \kappa_1 R_4^2 + \kappa_2 R_3^2 + \kappa_5 R_1^2 + \kappa_5' R_2^2\right)R_4 + \kappa_6 R_3 R_1 R_2 e^{-i\Delta}, \tag{28}$$

where

$$\Delta = \phi_3 + \phi_4 - \phi_1 - \phi_2. \tag{29}$$

Solutions of the system Eqs. (25)–(28) are invariant to arbitrary shifts of the phases ϕ_j $(j = 1, \ldots, 4)$, such that the combination Eq. (29) is not changed.

Taking into account the symmetries of the system Eqs. (25)–(28) here as in the case of square lattice we obtain six types of solutions: (i) traveling rolls (TR), (ii) standing rolls (SR), (iii) traveling rectangles (TRa), (iv) standing rectangles (SRa), (v) alternating rolls (rectangular) (AR-R), and (vi) standing cross-rolls (rectangular) (SCR-R).

The "standard" patterns as rolls and squares are more widespread than the rectangular ones, but without the latter ones the picture of the pattern selection is not complete. We have found the stability region of AR-R, applying the following criteria (see the Appendix):

(i) $\kappa_{1,r} + \kappa_{2,r} + \kappa_{5,r} + \kappa'_{5,r} - \kappa_{6,r} < 0$,
(ii) $\kappa_{1,r} - \kappa_{2,r} + \kappa_{5,r} - \kappa'_{5,r} + \kappa_{6,r} < 0$,
(iii) $\kappa_{1,r} - \kappa_{2,r} - \kappa_{5,r} + \kappa'_{5,r} + \kappa_{6,r} < 0$,
(iv) $\kappa_{1,r} + \kappa_{2,r} - \kappa_{5,r} - \kappa_{5,r} + 3\kappa_{6,r} < 0$,
(v) $-\mathrm{Re}[(\kappa_1 + \kappa_2 - \kappa_5 - \kappa_5')\kappa_{6,i}] - |\kappa_6|^2 < 0$.

The results presented in Fig. 2 show how the domain of stability of AR-R depends on the angle θ as well as on parameters characterizing the nonlinear behavior of the surface tension function on temperature (m_1 and m_2).The dotted lines on each panel of Fig. 2 show the previous results for the square lattice ($\theta = \pi/2$). Here the stable region is to the left from the lines. When the angle θ of the rhombic planform decreases then the region of AR-R stability shrinks (the solid line is for $\theta = 0.47\pi$, the dashed line is for $\theta = 0.45\pi$, and the dot-dashed line is for $\theta = 0.42\pi$). At $\theta = 0.4\pi$ all AR-R patterns become unstable. Figure 2(a) presents the linear surface tension ($m_1 = m_2 = 0$), Fig. 2(b) illustrates the case of $m_1 = 0.6m_0$ and $m_2 = 0$, Fig. 2(c) is for $m_1 = -0.5m_0$ and $m_2 = 0$, Fig. 2(d) is for $m_1 = 0.8m_0$ and $m_2 = -0.3$. The results show that the regime of ARs is preferred for the square lattice and very sensitive to the dependence of the surface tension on the temperature.

The domain of stability AR-R is not the only one at the rhombic lattice. At the angle θ close to $2\pi/3$ we can find stable traveling rectangles TRa2. Figure 3 shows the domains of stability of TRa2 at a rhombic lattice for different angles θ. As expected, the stable TRa2 domains depend on values of m_1 and m_2 and on the rhombic angle θ.

Figure 3(a) represents the case of linear surface tension (coefficients $m_1 = m_2 = 0$). Here the stable TRa2 structure appears at $\theta = 0.6\pi$ (green dot-dashed region), it grows with approaching of the θ to $2\pi/3$ (region depicted by dotted lines). Figure 3(b) is for $m_1 = 0.6m_0$ and $m_2 = 0$. Here the narrowed region of TRa2 appears at $\theta = 0.62\pi$. The negative value of coefficient m_1 on Fig. 3(c)

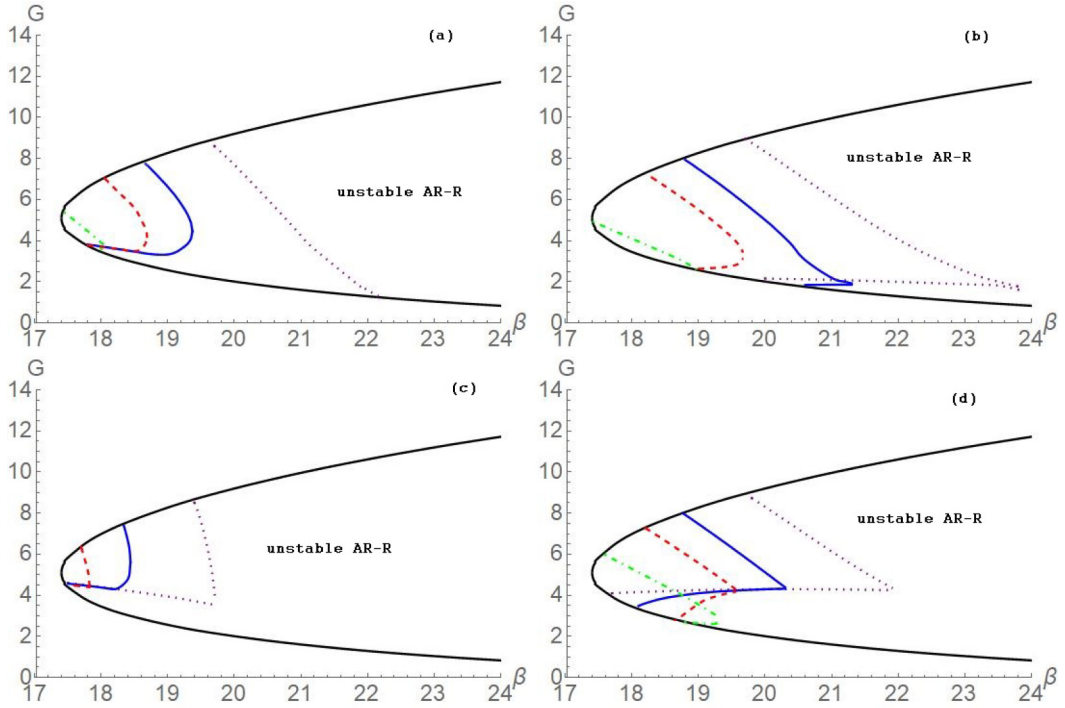

FIG. 2. Domains of stability for AR-R (left of the lines). The dotted line on each panel is for $\theta = \pi/2$ (square lattice), the solid line is for $\theta = 0.47\pi$, the dashed line is for $\theta = 0.45\pi$, and the dot-dashed green line 4 is for $\theta = 0.42\pi$. Here panel (a) $m_1 = 0.$, $m_2 = 0$; panel (b) $m_1 = 0.6m_0$, $m_2 = 0$; panel (c) $m_1 = -0.5m_0$, $m_2 = 0$, and panel (d) $m_1 = 0.8m_0$ and $m_2 = -0.3m_0$.

enlarges the region of the stable TRa2 structures (here $m_1 = -5m_0$). Figure 4(d) illustrates how the TRa2 domain shrinks at combination of the coefficients ($m_1 = 0.8m_0$ and $m_2 = -0.3m_0$).

C. Hexagonal patterns

The first order solution of the system of Eqs. (8) and (9) for the *hexagonal lattice* can be presented in the form:

$$h_1 = (A_1 e^{iKX} + A_2 e^{-iKX} + B_1 e^{(iK/2)(-X+\sqrt{3}Y)} + B_2 e^{(iK/2)(X-\sqrt{3}Y)} + C_1 e^{(iK/2)(-X-\sqrt{3}Y)} + C_2 e^{(iK/2)(X+\sqrt{3}Y)}) e^{i\omega_0 \tau_0} + \text{c.c.} \tag{30}$$

$$f_1 = \alpha(A_1 e^{iKX} + A_2 e^{-iKX} + B_1 e^{(iK/2)(-X+\sqrt{3}Y)} + B_2 e^{(iK/2)(X-\sqrt{3}Y)} + C_1 e^{(iK/2)(-X-\sqrt{3}Y)} + C_2 e^{(iK/2)(X+\sqrt{3}Y)}) e^{i\omega_0 \tau_0} + \text{c.c.} \tag{31}$$

Here $\alpha = 1 - 2(G + k^2\Sigma)/3m_0 - 2i\omega_0/m_0K^2$ and the wave vectors $\mathbf{K}_1 = (K, 0)$ and $\mathbf{K}_{2,3} = (-K/2, \pm\sqrt{3}K/2)$ form the basis of the hexagonal lattice, c.c. denotes complex conjugate terms.

Removing the resonant singularity of the nonlinear interaction at the third order we obtain the amplitude equations for the complex amplitudes $A_{1,2}$, $B_{1,2}$, and $C_{1,2}$:

$$\frac{dA_1}{d\tau_2} = (\kappa_0 + \kappa_1|A_1|^2 + \kappa_2|A_2|^2)A_1 + \kappa_7(|B_1|^2 + |C_1|^2)A_1 + \kappa_8(|B_2|^2 + |C_2|^2)A_1 + \kappa_9 A_2^*(B_1B_2 + C_1C_2), \tag{32}$$

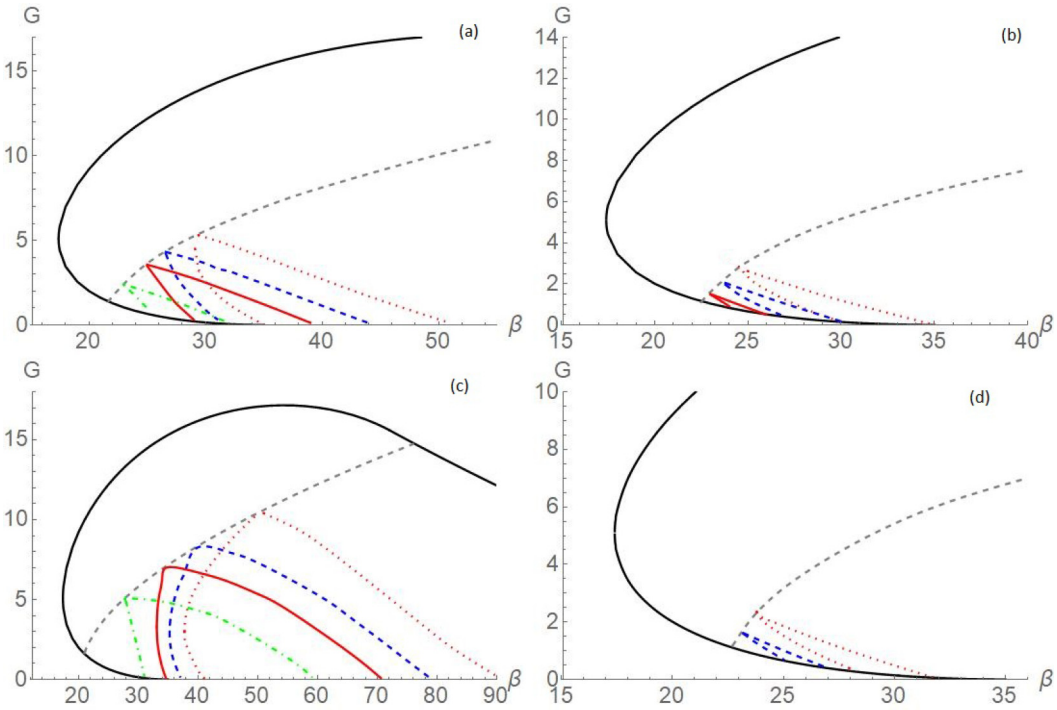

FIG. 3. Domains of stability for TRa2 at the rhombic lattice. Here the dotted lines shows the TRa2 domain at hexagonal lattice ($\theta = 2\pi/3$), blue dashed lines corresponds to $\theta = 0.64\pi$, the red solid region is for $\theta = 0.62\pi$, and green dot-dashed regions is for $\theta = 0.6\pi$. Panels: (a) linear surface tension, results of Shklyaev *et al.* [15]; (b) $m_1 = 0.6m_0$, $m_2 = 0$; (c) $m_1 = -0.5m_0$, $m_2 = 0$; (d) $m_1 = 0.8m_0$, $m_2 = -0.3m_0$. Above the gray dashed line on each panel TR bifurcates subcritically.

$$\frac{dA_2}{d\tau_2} = (\kappa_0 + \kappa_1|A_2|^2 + \kappa_2|A_1|^2)A_2 + \kappa_8(|B_1|^2 + |C_1|^2)A_2 + \kappa_7(|B_2|^2 + |C_2|^2)A_2 + \kappa_9 A_1^*(B_1B_2 + C_1C_2). \tag{33}$$

Other two pairs of amplitude equations for B_1, B_2, C_1, and C_2 can be obtained by cyclic permutations of A_j, B_j, and C_j ($j = 1, 2$). Here κ_7, κ_8, and κ_9 are complex coefficients and can be found as $\kappa_7 = \kappa_5(2\pi/3)$, $\kappa_8 = \kappa_5'(2\pi/3)$, and $\kappa_9 = \kappa_6(\pi/3)$.

Roberts, Swift, and Wagner [26] found 11 qualitatively different classes of bifurcating solutions; see Table II. A brief review of Ref. [26] and illustrations of these 11 limit cycles can be found in Ref. [3]. Other solutions can be obtained from these by symmetry transformations.

To determine whether solutions are subcritical or supercritical and whether supercritical are stable we have to evaluate some combinations of the coefficients of the system of Eqs. (32) and (33). Before carrying out the numerical stability analysis of the bifurcating solutions, we note that the traveling rectangles-1 (TRa1) are always unstable and stability properties of pairs (SH and SRT) and (TwR and WR2) cannot be distinguished in the framework of the cubic truncation Eqs. (32) and (33), the quintic order terms are needed; see Ref. [3]. Also we note that if TR solution is stable, then SR, OT, and TRa2 must be unstable.

To determine the stability of the patterns we use the following criteria:

(i) TR: $\kappa_{1,r} < 0$; $\kappa_{2,r} - \kappa_{1,r} < 0$; $\kappa_{7,r} - \kappa_{1,r} < 0$; $\kappa_{8,r} - \kappa_{1,r} < 0$;

(ii) SR: $\kappa_{1,r} + \kappa_{2,r} < 0$; $\kappa_{1,r} - \kappa_{2,r} < 0$; $-\kappa_{1,r} - \kappa_{2,r} + \kappa_{7,r} + \kappa_{8,r} < 0$; and $-|-\kappa_1 - \kappa_2 + \kappa_7 + \kappa_8|^2 + |\kappa_9|^2 < 0$;

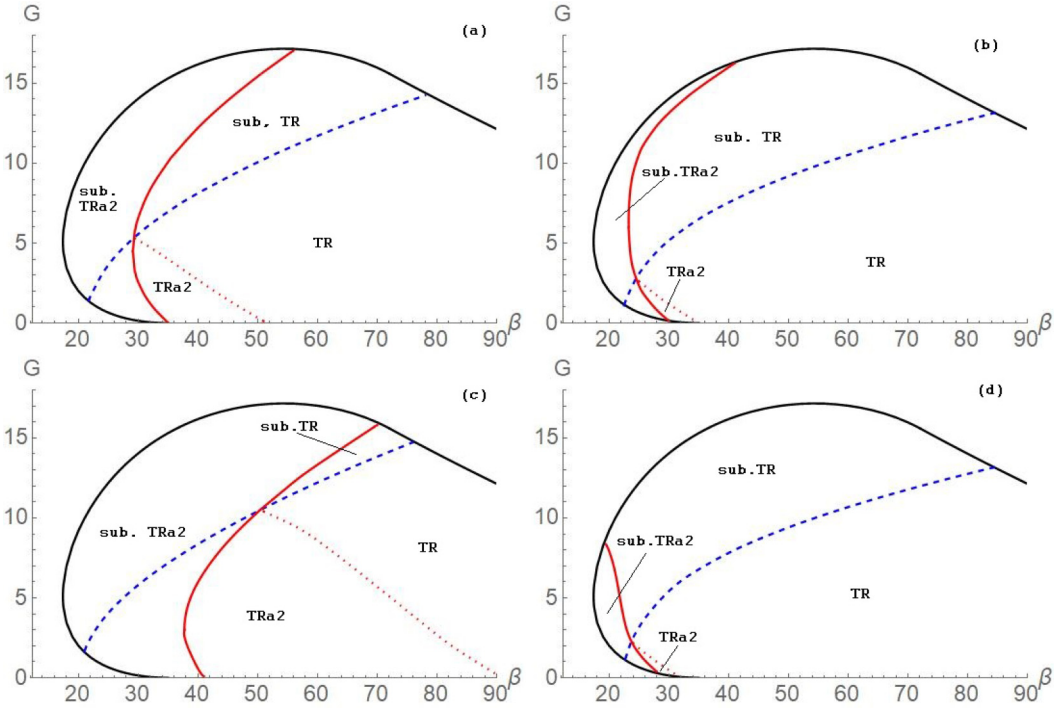

FIG. 4. Pattern selection of oscillatory mode on hexagonal lattice. Domains of stability for TR (below solid line and to the right of the dotted line) and TRa2 (below solid line and to the left to the dotted line). Panels: (a) linear surface tension, results of Shklyaev *et al.* [15]; (b) $m_1 = 0.6m_0$, $m_2 = 0$; (c) $m_1 = -0.5m_0$, $m_2 = 0$; (d) $m_1 = 0.8m_0$, $m_2 = -0.3m_0$.

(iii) OT: $\kappa_{1,r} + 2\kappa_{7,r} < 0$; $\kappa_{1,r} - \kappa_{7,r} < 0$; $-\kappa_{1,r} + \kappa_{2,r} - 2\kappa_{7,r} + 2\kappa_{8,r} + 2\kappa_{9,r} < 0$; $-\kappa_{1,r} + \kappa_{2,r} - 2\kappa_{7,r} + 2\kappa_{8,r} - \kappa_{9,r} < 0$;

(iv) WR1:$\kappa_{1,r} + \kappa_{2,r} + \kappa_{7,r} + \kappa_{8,r} - \kappa_{9,r} < 0$; $\kappa_{1,r} - \kappa_{2,r} + \kappa_{7,r} - \kappa_{8,r} + \kappa_{9,r} < 0$; $-\kappa_{1,r} - \kappa_{2,r} + \kappa_{7,r} + \kappa_{8,r} + \kappa_{9,r} < 0$; $\kappa_{1,r} - \kappa_{2,r} - \kappa_{7,r} + \kappa_{8,r} + \kappa_{9,r} < 0$; $\kappa_{1,r} + \kappa_{2,r} - \kappa_{7,r} - \kappa_{8,r} + 3\kappa_{9,r} < 0$; $-|\kappa_1 + \kappa_2 - \kappa_7 - \kappa_8 + 3\kappa_9|^2 + |\kappa_1 + \kappa_2 - \kappa_7 - \kappa_8 - \kappa_9|^2 < 0$;

TABLE II. The bifurcating solutions of Eqs. (32) and (33) found in Ref. [26].

(i) Standing rolls (SR)	$A_1 = A_2 \neq 0, B_1 = B_2 = C_1 + C_2 = 0$
(ii) Standing hexagons (SH)	$A_1 = A_2 = B_1 = B_2 = C_1 = C_2$
(iii) Standing regular triangles (SRT)	$A_1 = B_1 = C_1 = -A_2 = -B_2 = -C_2$
(iv) Standing triangles (ST)	$A_1 = B_1 = A_2 = B_2, C_1 = C_2 = 0,$
(v) Traveling rolls (TR)	$A_1 \neq 0, A_2 = B_1 = B_2 = C_1 = C_2 = 0$
(vi) Traveling rectangles-1 (TRa1)	$A_1 = C_1, A_2 = B_1 = B_2 = C_2 = 0$
(vii) Traveling rectangles-2 (TRa2)	$A_1 = C_2, A_2 = B_1 = B_2 = C_1 = 0$
(viii) Oscillating triangles (OT)	$A_1 = B_1 = C_1 \neq 0, A_2 = B_2 = C_2 = 0$
(ix) Wavy rolls-1 (WR1)	$A_1 = C_1 = A_2 = -C_2, B_1 = B_2 = 0$
(x) Twisted rectangles (TwR)	$A_1 = A_2, B_1 = B_2 = e^{2\pi i/3}A_1,$ $C_1 = C_2 = e^{4\pi i/3}A_1$
(xi) Wavy rolls-2 (WR2)	$A_1 = -A_2, B_1 = -B_2 = e^{2\pi i/3}A_1,$ $C_1 = e^{4\pi i/3}A_1 = -C_2$

(v) SH, SRT: $\kappa_{1,r}+\kappa_{2,r}+2\kappa_{7,r}+2\kappa_{8,r}+2\kappa_{9,r}<0$; $\kappa_{1,r}-\kappa_{2,r}+2\kappa_{7,r}-2\kappa_{8,r}-2\kappa_{9,r}<0$; $\kappa_{1,r}-\kappa_{2,r}-\kappa_{7,r}+\kappa_{8,r}-2\kappa_{9,r}<0$; $\kappa_{1,r}+\kappa_{2,r}-\kappa_{7,r}-\kappa_{8,r}-4\kappa_{9,r}<0$; $-|\kappa_1+\kappa_2-\kappa_7-\kappa_8-4\kappa_9|^2+|\kappa_1+\kappa_2-\kappa_7-\kappa_8+\kappa_9|^2<0$;

(vi) ST: $\kappa_{1,r}+\kappa_{2,r}+\kappa_{7,r}+\kappa_{8,r}+\kappa_{9,r}<0$; $\kappa_{1,r}-\kappa_{2,r}-\kappa_{7,r}+\kappa_{8,r}-\kappa_{9,r}<0$; $\kappa_{1,r}-\kappa_{2,r}+\kappa_{7,r}-\kappa_{8,r}-\kappa_{9,r}<0$; $-\kappa_{1,r}-\kappa_{2,r}+\kappa_{7,r}+\kappa_{8,r}-\kappa_{9,r}<0$; $\kappa_{1,r}+\kappa_{2,r}-\kappa_{7,r}-\kappa_{8,r}-3\kappa_{9,r}<0$; $|-\kappa_1-\kappa_2+\kappa_7+\kappa_8-\kappa_9|^2-4|\kappa_9|^2<0$; $-|\kappa_1+\kappa_2-\kappa_7-\kappa_8-3\kappa_9|^2+|\kappa_1+\kappa_2-\kappa_7-\kappa_8+\kappa_9|^2<0$;

(vii) TRa2: $\kappa_{1,r}+\kappa_{8,r}<0$; $\kappa_{1,r}-\kappa_{8,r}<0$; $\kappa_{7,r}-\kappa_{1,r}<0$; $-\kappa_{1,r}+\kappa_{2,r}+\kappa_{7,r}-\kappa_{8,r}+\kappa_{9,r}<0$; $-\kappa_{1,r}+\kappa_{2,r}+\kappa_{7,r}-\kappa_{8,r}-\kappa_{9,r}<0$;

(viii) TwR, WR2: $\kappa_{1,r}+\kappa_{2,r}+2\kappa_{7,r}+2\kappa_{8,r}-\kappa_{9,r}<0$; $\kappa_{1,r}-\kappa_{2,r}-\kappa_{7,r}+\kappa_{8,r}+\kappa_{9,r}<0$; $\kappa_{1,r}-\kappa_{2,r}+2\kappa_{7,r}-2\kappa_{8,r}+\kappa_{9,r}<0$; $\mathrm{Re}[T_1\pm\sqrt{T_1^2-T_2}]<0$; $T_1=\kappa_{1,r}+\kappa_{2,r}-\kappa_{7,r}-\kappa_{8,r}-\kappa_{9,r}+3\kappa_9^*$, $T_2=6\kappa_9^*(\kappa_1+\kappa_2-\kappa_7-\kappa_8-\kappa_9)$.

Here we consider the influence of the nonlinearity of surface tension function on the stability of the bifurcating solutions.

One of the results of work [15] was the existence of stable oscillatory traveling rectangles-2 (TRa2) on the hexagonal lattice. Figure 4(a) shows the selection of the oscillatory patterns on hexagonal lattice for case of linear surface tension function. The results are identical to those of Shklyaev *et al.* [15]. The dashed line is obtained using the condition $\kappa_{1,r}=0$ and it is a boundary between subcritical and supercritical TR solutions. The subcritical one is above this line and the supercritical solution is below. The stable TR domain on the hexagonal lattice is smaller than that on the square lattice (below the dashed line and to the right of the dotted one), because of the existence of TRa2 stability domain. TRa2 solution also can be subcritical (to the left of the solid red line) or supercritical (to the right of the solid red line), as well as stable (between the solid red line and the dotted line). In the case of nonlinearity at the positive values of coefficient m_1 and $n_2=0$, see Fig. 4(b), the region of the stable TR grows and the region of stable TRa2 shrinks. When the coefficient m_1 reverses its sign to the negative one we see the growth of the TRa2 region and decrease of the stable TR region; see Fig. 4(c). Figure 4(d) shows that by changing values of the coefficients m_1 and m_2 the region of the stable traveling rectangles-2 can disappear. Other patterns are unstable in a cubic truncation of nonlinearity and not considered in the frame of this work.

The same domains of stable TRa2 structures can be obtained at the rhombic lattice, in the case where $\theta=2\pi/3$ (see dotted lines in Fig. 3).

III. SUMMARY

The present work investigates a pattern selection in oscillatory longwave Marangoni convection in a heated thin layer of fluid with weak heat flux from the free surface. The novelty of our research is that the nonlinear dependence of the surface tension on the temperature is taken into consideration. A lot of experiments (for example, Refs. [16–21]) reveal this nonlinearity. The weakly nonlinear analysis of the set of amplitude equations describing a 3D Marangoni convection near stability threshold was carried out. The pattern selection was analyzed on square, rhombic and hexagonal lattices. Their domains of stability have been determined.

The selection that has been carried out on a square lattice demonstrates the possible existence of stable domains for the alternating (AR) and traveling (TR) rolls. The region of stability of TR exists for all considered cases of surface tension nonlinearity. The AR stability region shrinks or expands depending on the type of this nonlinearity. A small zone of bistability when both AR and TR patterns are stable is found. The pattern on the rhombic lattice is formed by interaction of two waves propagating under the angle θ on to another. This angle is additional parameter that influences the selection of patterns. The stability regions of AR-R depend on the angle θ. They exist only in the range between $\theta=\pi/2$ and 0.4π. The stability criteria of AR on the rhombic lattice are obtained. They are different comparing with the similar criteria on the square lattice. When θ is close to $2\pi/3$ the stable TRa2 region appears at the rhombic lattice. The appearance of TRa2 region strongly depends on the angle θ.

On the hexagonal lattice, together with the TR stability region, the stability of TRa2 appears. The stability regions of the traveling rectangles on the hexagonal lattice equals to regions of stable TRa2 at the rhombic lattice despite the additional stability criteria. When TR stable region increases, the TRa2 stable region decreases.

The subject of this paper was investigation of the pattern selection in the oscillatory Marangoni convection in the layer heated from below, discovered by Shklyaev *et al.* [15]. This oscillatory instability has not yet been observed in experiments. Here we try to present the experimental conditions for its possible observation. Assuming we have layer of aqueous long chain alcohol solution, like in Ref. [19], with thickness of 0.01 cm, surface tension 40 dyn/cm, kinetic viscosity 0.1 cm^2/s, thermal diffusivity $\chi = 0.005\ \mathrm{cm}^2/\mathrm{s}$, and density 0.8 $\mathrm{g/cm}^3$. This results in the Galileo number $G \sim 2$ and the inverse capillary number $S \sim 1000$; assuming $q = 5\ \mathrm{W/m}^2\mathrm{K}$ we have $\mathrm{Bi} \sim 0.004$. The characteristic wavelength of the convective structure is $d_0/\sqrt{\mathrm{Bi}} \sim 1.6$ mm and the critical temperature difference is 20 K. Similar estimations for the thickness of the layer 0.05 mm in Ref. [15] give the attained critical Marangoni number at temperature difference 0.5 K. In Ref. [27] authors considered two-layer system with 1 mm air layer over the 0.1 mm film of silicon. For this configuration the critical Marangoni number is attained at temperature difference 4 K.

ACKNOWLEDGMENT

A.A.N. acknowledges the support by the Israel Science Foundation (Grant No. 843/18).

APPENDIX: STABILITY CRITERIA OF ALTERNATING ROLLS

The alternating rolls (AR-R) are described by the solution of Eqs. (25)–(29),

$$R_1 = R_2 = R_3 = R_4 = a, \quad \Delta = \pi, \quad a^2 = -\frac{\kappa_{0,r}}{\kappa_{1,r} + \kappa_{2,r} + \kappa_{5,r} + \kappa'_{5,r} - \kappa_{6,r}}. \tag{A1}$$

Linearizing Eqs. (25)–(29) around AR-R solution and taking into account Eq. (A1) we obtain the eigenvalue problem for the eigenvector $(\tilde{R}_1, \tilde{R}_2, \tilde{R}_3, \tilde{R}_4, \tilde{\Delta})$ and eigenvalue r (growth rate):

$$\begin{aligned}&[-r + (2\kappa_{1,r} + \kappa_{6,r})a^2]\tilde{R}_1 + (2\kappa_{2,r} - \kappa_{6,r})a^2\tilde{R}_2 + (2\kappa_{5,r} - \kappa_{6,r})a^2\tilde{R}_3 + \dots \\ &\quad + (2\kappa'_{5,r} - \kappa_{6,r})a^2\tilde{R}_4 + \kappa_{6,i}a^3\tilde{\Delta} = 0,\end{aligned} \tag{A2}$$

$$\begin{aligned}&(2\kappa_{2,r} - \kappa_{6,r})a^2\tilde{R}_2 + [-r + (2\kappa_{1,r} + \kappa_{6,r})a^2]\tilde{R}_2 + (2\kappa'_{5,r} - \kappa_{6,r})a^2\tilde{R}_3 + \dots \\ &\quad + (2\kappa_{5,r} - \kappa_{6,r})a^2\tilde{R}_4 + \kappa_{6,i}a^3\tilde{\Delta} = 0,\end{aligned} \tag{A3}$$

$$\begin{aligned}&(2\kappa_{5,r} - \kappa_{6,r})a^2\tilde{R}_1 + (2\kappa'_{5,r} - \kappa_{6,r})a^2\tilde{R}_2 + [-r + (2\kappa_{1,r} + \kappa_{6,r})a^2]\tilde{R}_3 + \dots \\ &\quad + (2\kappa_{2,r} - \kappa_{6,r})a^2\tilde{R}_4 - \kappa_{6,i}a^3\tilde{\Delta} = 0,\end{aligned} \tag{A4}$$

$$\begin{aligned}&(2\kappa'_{5,r} - \kappa_{6,r})a^2\tilde{R}_1 + (2\kappa_{5,r} - \kappa_{6,r})a^2\tilde{R}_2 + (2\kappa_{2,r} - \kappa_{6,r})a^2\tilde{R}_3 + \dots \\ &\quad + [-r + (2\kappa_{1,r} + \kappa_{6,r})a^2]\tilde{R}_4 - \kappa_{6,i}a^3\tilde{\Delta} = 0,\end{aligned} \tag{A5}$$

$$2(\kappa_{1,i} + \kappa_{2,i} - \kappa_{5,i} - \kappa'_{5,i} + \kappa_{6,i})a(\tilde{R}_1 + \tilde{R}_2 - \tilde{R}_3 - \tilde{R}_4) + (r - 4\kappa_{6,r}a^2)\tilde{\Delta} = 0. \tag{A6}$$

Due to the symmetry of the system, all the eigenvectors belong to the following four classes: (i) $\tilde{R}_1 = \tilde{R}_2 = \tilde{R}_3 = \tilde{R}_4$; (ii) $\tilde{R}_1 = \tilde{R}_2 = -\tilde{R}_3 = -\tilde{R}_4$; (iii) $\tilde{R}_1 = -\tilde{R}_2 = \tilde{R}_3 = -\tilde{R}_4$; (iv) $\tilde{R}_1 = -\tilde{R}_2 = -\tilde{R}_3 = \tilde{R}_4$.

In case (i), we obtain the stability condition

$$\kappa_{1,r} + \kappa_{2,r} + \kappa_{5,r} + \kappa'_{5,r} - \kappa_{6,r} < 0, \tag{A7}$$

which is condition of the supercritical bifurcation, $\kappa_{0,r} > 0$.

In case (ii), we get two stability conditions:

$$\kappa_{1,r} + \kappa_{2,r} - \kappa_{5,r} - \kappa'_{5,r} + 3\kappa_{6,r} < 0, \tag{A8}$$

$$-|\kappa_6|^2 - \mathrm{Re}[\kappa_{3,i}(\kappa_{1,r} + \kappa_{2,r} - \kappa_{5,r} - \kappa'_{5,r})] < 0, \tag{A9}$$

which determine the boundaries of the oscillatory and monotonic instability, respectively.

Case (iii) leads the following stability condition:

$$\kappa_{1,r} - \kappa_{2,r} + \kappa_{5,r} - \kappa'_{5,r} + \kappa_{6,r} < 0, \tag{A10}$$

and case (iv) gives us the condition

$$\kappa_{1,r} - \kappa_{2,r} - \kappa_{5,r} + \kappa'_{5,r} + \kappa_{6,r} < 0. \tag{A11}$$

If $\kappa_{5,r} = \kappa'_{5,r}$, then the conditions obtained by Silber and Knobloch [25] are reproduced (condition Eqs. (A10) and (A11) coincide in that case).

[1] M. C. Cross and P. C. Hohenberg, Pattern formation outside of equilibrium, Rev. Mod. Phys. **65**, 851 (1993).

[2] M. Golubitsky, J. W. Swift, and E. Knobloch, Symmetries and pattern selection in Rayleigh-Bénard convection, Physica D **10**, 249 (1984).

[3] T. Clune and E. Knobloch, Pattern selection in three-dimensional magnetoconvection, Physica D **74**, 151 (1994).

[4] M. D. Groves, D. J. B. Lloyd, and A. Stylianou, Pattern formation on the free surface of a ferrofluid: Spatial dynamics and homoclinic bifurcation, Physica D **350**, 1 (2017).

[5] M. Silber and E. Knobloch, Pattern selection in steady binary-fluid convection, Phys. Rev. A **38**, 1468 (1988).

[6] P. Shukla and M. Alam, Nonlinear stability and patterns in granular Couette flow: Hopf and pitchfork bifurcations, and evidence for resonance, J. Fluid Mech. **672**, 147 (2011).

[7] L. Yang, A. M. Zhabotinsky, and I. R. Epstein, Stable Squares and Other Oscillatory Turing Patterns in a Reaction-Diffusion Model, Phys. Rev. Lett. **92**, 198303 (2004)

[8] J. W. Scanlon and L. E. Segel, Finite-amplitude cellular convection induced by surface tension, J. Fluid Mech. **30**, 149 (1962).

[9] J. R. Pearson, On convection cells induced by surface tension, J. Fluid Mech. **4**, 489 (1958).

[10] L. E. Scriven and C. V. Sternling, On cellular convection driven by surface-tension gradients: Effects of mean surface tension and surface viscosity, J. Fluid Mech. **19**, 321 (1964).

[11] G. I. Sivashinsky, Large cells in nonlinear Marangoni convection, Physica D **4**, 227 (1982).

[12] E. Knobloch, Pattern selection in long-wavelength convection, Physica D **41**, 450 (1990).

[13] S. H. Davis, Rupture of thin liquid films, in *Waves on Fluid Interfaces*, edited by R. E. Mayer (Academic Press, New York, 1983), p. 291.

[14] A. A. Golovin, A. A. Nepomnyashchy, and L. M. Pismen, Pattern formation in large-scale Marangoni convection with deformable interface, Physica D **81**, 117 (1995).

[15] S. Shklyaev, A. A. Alabuzhev, and M. Khenner, Long-wave Marangoni convection in a thin film heated from below, Phys. Rev. E **85**, 016328 (2012).

[16] G. Petre, M. A. Azouni, and K. Tshinyama, Marangoni convection at alcohol aqueous solutions-air interfaces, App. Sci. Res. **50**, 97 (1993).

[17] J. C. Legros, M. C. Limbourg-Fontaine, and G. Petre, Influence of a surface tension minimum as a function of temperature on the Marangoni convection, Acta Astronaut. **11**, 143 (1984).

[18] M. C. Limbourg-Fontaine, G. Petre, J. C. Legros, and E. Van Ransbeeck, Thermocapillary movements around a surface tension minimum under microgravity conditions (Part 1. Technical description of STEM experiments. D_1 mission of Spacelab, Acta Astronaut. **13**, 197 (1986).

[19] J. C. Legros, Problems related to nonlinear variations of surface tension, Acta Astronaut. **13**, 697 (1986).
[20] N. Eustathopoulos, J. C. Joud, P. Desre, and J. M. Hicter, The wetting of carbon by aluminium and aluminium alloys, J. Mater. Sci. **9**, 1233 (1974).
[21] D. Villers and J. K. Platten, Thermal convection in superposed immerscible liquid layers, Appl. Sci. Res. **45**, 145 (1988).
[22] A. B. Mikishev and A. A. Nepomnyashchy, Influence of nonlinear thermocapillary effect on Marangoni patterns in thin film, Phys. Rev. Fluids **5**, 054001 (2020).
[23] G. Z. Gershuni and E. M. Zhukhovitskii, *Convective Stability of Incompressible Fluids* (Keter, Jerusalem, 1976).
[24] See Supplemental Material at http://link.aps.org/supplemental/10.1103/PhysRevFluids.6.014002 for expressions of κ_i (here $i = 1, 2, 3, 4, 5, 6$).
[25] M. Silber and E. Knobloch, Hopf bifurcation on a square lattice, Nonlinearity **4**, 1063 (1991).
[26] M. Roberts, J. W. Swift, and D. H. Wagner, The Hopf bifurcation on a hexagonal lattice, in *Multiparameter Bifurcation Theory*, edited by M. Golubitsky and J. M. Guckenheimer, AMS Series: Contemporary Mathematics Vol. 56 (AMS, Providence, RI, 1986), pp. 283–318.
[27] A. E. Samoilova and S. V. Shklyaev, Oscillatory Marangoni convection in a liquid-gas system heated from below, Eur. Phys. J: Spec. Top. **224**, 241 (2015).